

Ultra-High Sensitive NO₂ Gas Sensor Based on Tunable Polarity Transport in CVD-WS₂/IGZO p-N Heterojunction

Tang, Hongyu; Li, Yutao; Sokolovskij, Robert; Sacco, Leandro; Zheng, Hongze; Ye, Huaiyu; Yu, Hongyu; Fan, Xuejun; Zhang, Guoqi; More Authors

DOI

[10.1021/acsami.9b13773](https://doi.org/10.1021/acsami.9b13773)

Publication date

2019

Document Version

Final published version

Published in

ACS Applied Materials and Interfaces

Citation (APA)

Tang, H., Li, Y., Sokolovskij, R., Sacco, L., Zheng, H., Ye, H., Yu, H., Fan, X., Zhang, G., & More Authors (2019). Ultra-High Sensitive NO₂ Gas Sensor Based on Tunable Polarity Transport in CVD-WS₂/IGZO p-N Heterojunction. *ACS Applied Materials and Interfaces*, 11(43), 40850-40859. <https://doi.org/10.1021/acsami.9b13773>

Important note

To cite this publication, please use the final published version (if applicable). Please check the document version above.

Copyright

Other than for strictly personal use, it is not permitted to download, forward or distribute the text or part of it, without the consent of the author(s) and/or copyright holder(s), unless the work is under an open content license such as Creative Commons.

Takedown policy

Please contact us and provide details if you believe this document breaches copyrights. We will remove access to the work immediately and investigate your claim.

Ultra-High Sensitive NO₂ Gas Sensor Based on Tunable Polarity Transport in CVD-WS₂/IGZO p-N Heterojunction

Hongyu Tang,^{†,‡,§,||} Yutao Li,^{‡,||} Robert Sokolovskij,^{†,||} Leandro Sacco,^{†,||} Hongze Zheng,^{||} Huaiyu Ye,^{*,||,⊥} Hongyu Yu,^{||} Xuejun Fan,[#] He Tian,^{‡,||} Tian-Ling Ren,^{*,‡} and Guoqi Zhang^{*,†}

[†]Department of Microelectronics, Delft University of Technology, Delft 2628 CD, The Netherlands

[‡]Institute of Microelectronics, Beijing National Research Center for Information Science and Technology (BNRist), Tsinghua University, Beijing 100084, China

[§]Changzhou Institute of Technology Research for Solid State Lighting, Changzhou 213161, China

^{||}School of Microelectronics, Southern University of Science and Technology, Shenzhen 518055, China

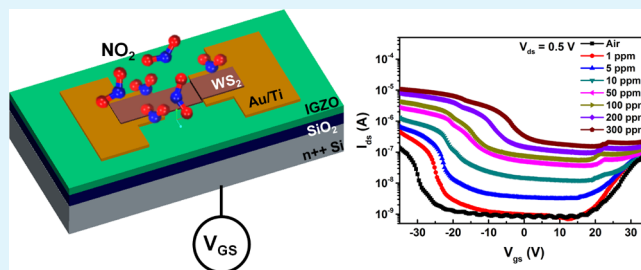
[⊥]Shenzhen Institute of Wide-bandgap Semiconductors, Shenzhen 518055, China

[#]Department of Mechanical Engineering, Lamar University, Beaumont, Texas 77710, United States

Supporting Information

ABSTRACT: In this work, a thin-film transistor gas sensor based on the p-N heterojunction is fabricated by stacking chemical vapor deposition-grown tungsten disulfide (WS₂) with a sputtered indium–gallium–zinc-oxide (IGZO) film. To the best of our knowledge, the present device has the best NO₂ gas sensor response compared to all the gas sensors based on transition-metal dichalcogenide materials. The gas-sensing response is investigated under different NO₂ concentrations, adopting heterojunction device mode and transistor mode. High sensing response is obtained of p-N diode in the range of 1–300 ppm with values of 230% for 5 ppm and 18 170% for 300 ppm. On the transistor mode, the gas-sensing response can be modulated by the gate bias, and the transistor shows an ultrahigh response after exposure to NO₂, with sensitivity values of 6820% for 5 ppm and 499 400% for 300 ppm. Interestingly, the transistor has a typical ambipolar behavior under dry air, while the transistor becomes p-type as the amount of NO₂ increases. The assembly of these results demonstrates that the WS₂/IGZO device is a promising platform for the NO₂-gas detection, and its gas-modulated transistor properties show a potential application in tunable engineering for two-dimensional material heterojunction-based transistor device.

KEYWORDS: WS₂/IGZO, p-N heterojunction, gas sensing, NO₂, TFT, ambipolar



1. INTRODUCTION

Two-dimensional (2D) transition-metal dichalcogenides (TMDCs) have attracted great attention due to their unique physical and chemical properties and their development in a wide variety of applications.^{1–6} Tungsten sulfide (WS₂), as a typical TMDC material, is a semiconductor with a S–W–S sandwich structure and an indirect band gap of ~1.9 eV. These features enable WS₂ to have great potential for transistor, photodetector, solar cell, and gas sensor applications.^{7–9} Theoretical studies based on density functional theory calculations show that adsorbed molecules on the monolayer and few layer WS₂ can change the band gap, thereby further modulating its electronic and optical properties.^{10,11} Based on theoretical works, researchers have been encouraged to fabricate WS₂-based gas sensors to detect NO₂ and NH₃. Xu et al.¹² synthesized ultrathin WS₂ nanosheets through the hydrothermal and calcination process, which showed a high response of 9.3% after exposure to 0.1 ppm NO₂ gas at room temperature (RT). Ko et al.¹³ proposed a gas sensor for

detecting acetone and NO₂ based on large area WS₂ nanosheets which were synthesized by sulfurizing the deposited WO₃ atomic layer. The response after exposure to 500 ppm NO₂ gas was about 16% but with incomplete recovery. The liquid phase exfoliated WS₂ flake-based gas sensor showed p-type sensing behavior and excellent detection limits in dry air for NH₃ and NO₂ (1 ppm and 100 ppb, respectively) operationally at 150 °C.¹⁴ However, the gas response is not very high and the device cannot work well at RT.

To overcome the intrinsic shortcomings of pure WS₂ nanomaterials and improve its sensing behavior, TMDC-based heterojunctions that are constructed with two or more semiconductors have been proposed. In general, a slight external disturbance, such as an electric field, illumination,

Received: August 7, 2019

Accepted: October 2, 2019

Published: October 2, 2019

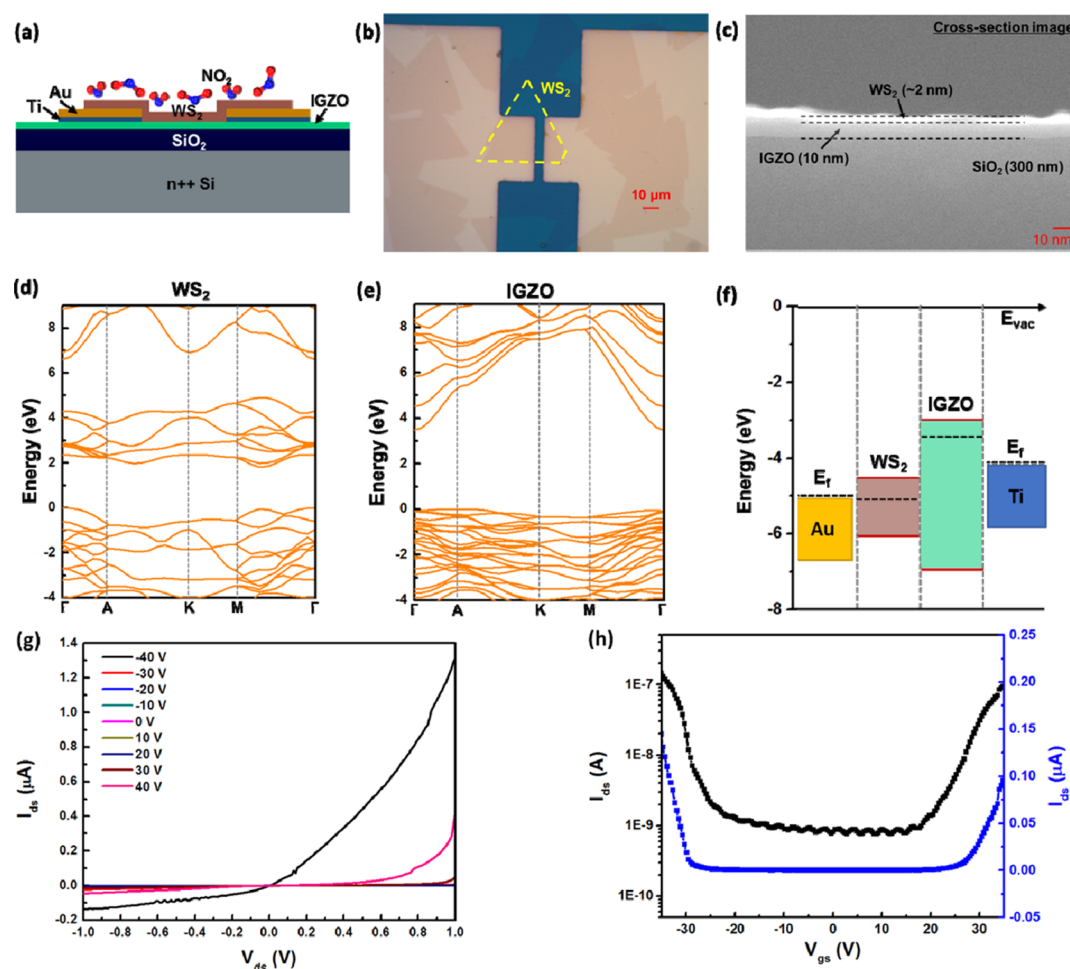


Figure 1. (a) Schematic diagram of the WS₂/IGZO heterojunction transistor. (b) Optical image, (c) SEM cross sections of the WS₂/IGZO heterojunction. Band structure of (d) WS₂ and (e) IGZO with first-principles calculations. (f) Calculated band alignment between WS₂ and IGZO, and the position of work function of Au. The black dashed lines represent the Fermi level, indicating the small contact barrier. (g) Output characteristics of the device, showing the symmetrical ambipolar behavior ($V_{ds} = 0-1$ V, $V_{gs} = -40$ to 40 V). (h) Transfer characteristics during the period of sweeping gate voltage in linear (black line) and logarithmic (blue line) scales ($V_{ds} = 0.5$ V, $V_{gs} = -40$ to 40 V).

strain, and gas adsorption, can induce intensive electric transport at the interface between two contact layers.¹⁵ Thus, Perrozzi et al.¹⁴ fabricated a NO₂ gas sensor based on the WS₂/WO₃ hierarchical structure that exhibited a limit of detection (LOD) of 100 ppm at 150 °C operation temperature. Yan et al.¹⁶ proposed a WS₂/graphene aerogel (GA) device for increasing the selectivity to a specific gas under different humidity and temperature atmosphere. Because NO₂ molecules can accept electrons from GA, the potential barrier between graphene and WS₂ decreases, and finally results in high selectivity to NO₂ with a LOD of 10 ppb at RT under 60% RH. Compared with the pure TMDC-based gas sensor, the TMDCs/metal oxide-based p-n heterojunction device can effectively overcome the shortcoming of long response times and high working temperatures. Generally, a depletion region and bands bending occurs in the contact sections of the p-n junction, which directly induces great variation of the conductivity and acceleration of the response and recovery times. Regarding the device response, field-emission transistor (FET) provides an outstanding platform to improve device sensitivity because it is characterized by gate-tunable electronic properties. Therefore, three terminal devices are more suitable for ultrasensitive devices. For instance, Tabata et al.¹⁷ fabricated a gate-tunable gas sensor based on a graphene/

MoS₂ van der Waals heterojunction, which had a high response to NO₂ of 10³, and the magnitude of the response strongly dependent on the bias and back-gate voltages. Bae et al.¹⁸ demonstrated a dual-channel gas sensor based on the ZnO/graphene hybrid heterostructure transistor, which showed superior response than most of the graphene-based gas sensors. Because the interaction between the gas molecule and sensitive layer (the FET channel material) enable an obvious electron transfer between them, which can further change the carrier concentration, mobility, and semiconductor work function of the device, and finally affect the transistor current.^{19,20} However, the majority of three-terminal gas sensors are based on one- or two-dimensional FETs, which their implementation for large-scale production is severely limited.²¹

In contrast, thin-film transistors (TFTs) are widely used in many emerging display technologies,²² particularly, indium-gallium-zinc-oxide (IGZO), is one of the most promising oxide semiconductors for TFTs and it is replacing amorphous silicon in display drivers.²³ IGZO, a typical metal-oxide complex semiconductor, has a wide band gap (~3.5 eV at 300 K),²⁴ high carrier mobility (~35.8 cm²/V s),²⁵ low-temperature processing features,²⁶ and outstanding stability.²⁷ Thus, high-performance TFT-type NO₂ gas sensors that use IGZO as the channel material were successfully fabricated by a

few researchers.^{19,28} Thus, many efforts have been devoted to systematically study gas sensors directly utilizing amorphous oxide TFTs. Collectively, both of WS₂ and IGZO has a graphene-like structure, and most of metal-oxide substrates can enable an increase of charge exchanges between the interface, IGZO would therefore be advantageous for enhancing the electrical, optical, and sensing properties of the WS₂.^{29,30}

In the present work, the TFT gas sensor based on the p-N heterojunction is fabricated by vertically stacking the sputtered amorphous IGZO film and 2D WS₂ film synthesized by chemical vapor deposition (CVD). The performance of the CVD-WS₂/IGZO gas sensor device under different NO₂ gas concentration is investigated by adopting two different device configurations: chemiresistor and TFT mode. In both cases, the mechanisms involved in the sensing process are deeply discussed using the theory of the electronic band. The present article aims to provide a new stacked heterojunction for ultrasensitive NO₂ gas sensing and tunable engineering application.

2. EXPERIMENTAL SECTION

2.1. Device Fabrication. An IGZO film (10 nm) was deposited onto an n++ type Si/SiO₂ substrate through RF magnetron sputtering. Then, source/drain (S/D) electrodes were formed through thermal evaporation of Ti (10 nm)/Au (30 nm). After the photolithographic lift-off process, an IGZO TFT was obtained. To fabricate a WS₂/IGZO heterojunction TFT, the monolayer WS₂ film grown by the CVD process was transferred onto the fixed position of the IGZO surface and covered on the top of S/D electrodes by using a poly(methyl methacrylate) (PMMA) supporting layer with a custom fixture. Finally, the PMMA was removed by dipping in acetone for 10 min and ethanol for 5 min. For comparison, we also fabricated a WS₂ TFT, whose procedure is similar to that of the WS₂/IGZO heterojunction TFT except for the deposition of the IGZO film. The schematics of WS₂ TFT, IGZO TFT, and WS₂/IGZO heterojunction TFT are shown in the inset image of Figures S1a,b and 1a, respectively.

2.2. Characterization. The optical microscopy images were obtained from an optical microscope (OLYMPUS TH4-200) imager with white light illumination. The thickness of CVD-WS₂ and IGZO were measured by using an atomic force microscope (AFM, Bruker, Santa Barbara, CA, USA). The Raman and photoluminescence (PL) spectra of the WS₂, IGZO, and WS₂/IGZO heterojunction were obtained through a Raman spectroscopy meter (Raman, HORIBA, LabRAM HR Evolution) excited by a 532 nm laser. The film morphology was characterized by field-emission scanning electron microscopy (SEM; SUPRA 55VP, Carl Zeiss, Germany).

2.3. Gas Test. For the investigation of the effects of gas on the electronic properties of the WS₂/IGZO heterostructure on SiO₂, experiments were performed in the DGL-III Testing System (Beijing Elite Tech Co., Ltd) with the atmospheric conditions changing in the following order: dry air, gradually increasing NO₂ concentration, and dry air. All the gas-sensing experiments were carried out at RT and room atmospheric pressure. Figure S2 shows the experimental setup used for gas-sensing performance.

2.4. Electrical Characterization. Mott–Schottky measurements were performed on a CHI660C electrochemical workstation using a three-electrode cell system. In this measurement, 0.5 M Na₂SO₄ was used as the electrolyte, while WS₂, platinum, and Ag/AgCl were used as the cathode, anode, and reference electrode, respectively. The frequency was fixed at 1 kHz. Electrical characterization of the WS₂/IGZO heterojunction device was performed by using an electrical analysis system (two Keithley 2450 SourceMeter, one for supplying drain–source voltage (V_{ds}), and the other for supplying gate–source voltage (V_{gs}) to record the real-time current change (data acquisition time ~30 ms) using a three-probe in the gas chamber. Before the gas-sensing test, the WS₂/IGZO-based devices were stabilized in air in the

system for about 30 min to fully restore to the initial state. The current–voltage (I_{ds} – V_{ds}) measurements were taken from –1 to +1 V. The transfer characteristics (I_{ds} – V_{gs}) were recorded with a constant V_{ds} of 0.5 V. The transistor electrical parameters, namely, the field-effect mobility (μ), threshold voltage (V_{th}), and on/off current ratio (I_{on}/I_{off}), were extracted from the characteristic curves in the saturation regime. The sensing performance of the WS₂/IGZO heterojunction was evaluated according to the response (S) and response time. Here, S is defined by the relative current change, as the percent change in current divided by the initial current in different gas concentrations.

$$S = (I_{g(V_{gs})} - I_{0(V_{gs})})/I_{0(V_{gs})} \times 100\% \quad (1)$$

where $I_{g(V_{gs})}$ and $I_{0(V_{gs})}$ are the drain–source current of the device upon the introduction of NO₂ gas and in dry air under different V_{gs} , respectively. When $V_{gs} = 0$ V, S is the response on the chemiresistor mode; when $V_{gs} \neq 0$ V, S is the response on the transistor mode.

3. RESULTS AND DISCUSSION

3.1. Characterization and Electrical Transport Properties of the WS₂/IGZO Heterojunction Device. Figure 1a–c shows the schematic diagram, optical, and SEM images of the WS₂/IGZO device structure, respectively. The device has a channel length of 5 μ m and width of 20 μ m. The top surface of IGZO contact with the Ti metal layer and the bottom surface of WS₂ contact with the Au film, which affects the band alignment of the semiconductor materials and metals. The AFM scanning images of WS₂ and IGZO films are shown in Figure S3a,b, respectively. It can be found that the height of the WS₂ is ~1.2 nm, indicating that it is a monolayer WS₂.⁵ As shown in Figure S4, the Raman spectra for both WS₂/IGZO and WS₂ have two main bands at 354 and 419 cm^{–1}, which correspond to the E_{2g}¹ and A_{1g} modes of the WS₂ crystal.³⁰ It indicates that the transferring process in both substrates (IGZO and SiO₂) is equivalent. Moreover, the PL intensity of the heterojunction is lower than that of WS₂, which further confirms that the electrons and holes generated from separated excitons transferred from WS₂ and IGZO effectively.³¹

To explain the contact barrier between semiconductors and Ti/Au metal in more detail, we analyzed the band structures of WS₂ and IGZO and the work functions of Ti, Au through first-principles calculations. Figure 1d,e shows the calculated band structures of WS₂ and IGZO crystals, respectively. The band diagram structure provides the band gap values of the metal electrodes to estimate the type-I band alignment between WS₂ and IGZO as well as the position of Au and Ti work functions, as shown in Figure 1f. WS₂ has a narrower band gap, whose Fermi level (E_f) is almost equal to that of Au and much lower than that of IGZO. Concerning the Ti, their E_f is lower than that of IGZO. It indicates that the contact barrier between Au and WS₂ is small and negligible, while the barrier between Ti and IGZO is large and positive. Thus, the I – V curve under an air environment shows rectification characteristics consisting of an Au/WS₂ near-Ohmic contact and Ti/IGZO Schottky contact (see Figures 1g and S5). In this work, WS₂ shows a p-type semiconductor nature according to the Mott–Schottky plot drawn between $1/C^2$ and the potential with respect to the saturated calomel electrode (SCE) (see Figure S6). The flat band potential (E_{FB}) is found to be 0.43 V_{SCE} with acceptor density (N_A) in the range of $9.8 \times 10^{17}/\text{cm}^3$, which agrees with the reported value (0.45 V_{SCE} with N_A of $10^{18}/\text{cm}^3$ by Tonti et al.,³² and 0.44 V_{SCE} with N_A of $9.7 \times 10^{17}/\text{cm}^3$ by Devadasan et al.³³). Accordingly, three regions of the device configuration,

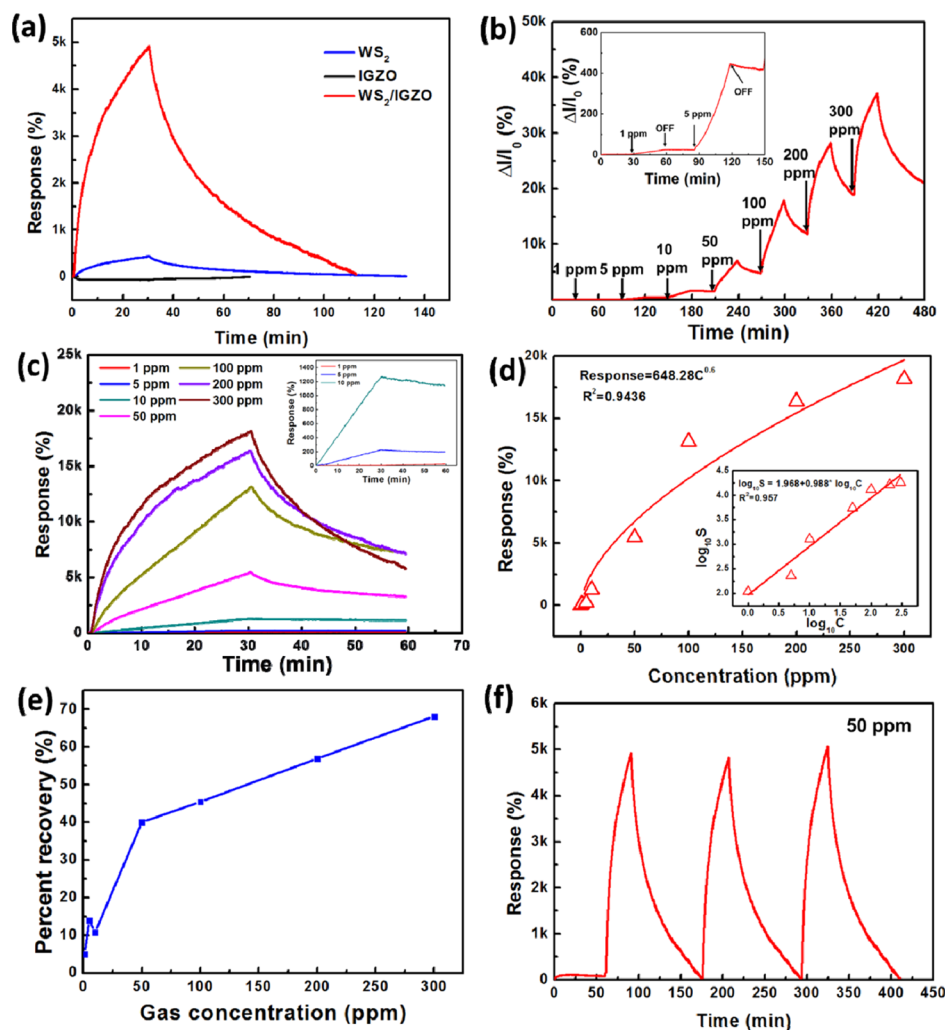


Figure 2. (a) Response of IGZO-only, WS₂-only, and WS₂/IGZO devices after exposure to 50 ppm NO₂. (b) Real time response of a WS₂/IGZO device after exposure to NO₂ under different concentrations. Inset image is the magnified curve of current change under 1 and 5 ppm NO₂ gas concentration. (c) Response of the device after exposure to NO₂ under different concentrations. Inset image is the magnified curve of normalized response under 1, 5, and 10 ppm NO₂ gas concentration. (d) Response vs NO₂ concentrations fitted by using the Freundlich isotherm adsorption model. Inset: $\log_{10} S$ vs $\log_{10} C$ with linear line fitting. (e) Percent recovery of the device after exposure to NO₂ under different concentrations. (f) Dynamic response of a sensor during 3 successive cycles of exposure to 50 ppm NO₂. All the test were carried out at RT.

including heterojunction, p-channel of WS₂, and n-channel of IGZO, can dominate the electrical transport of the systems.

According to its output (Figure 1g) and transfer (Figure 1h) characteristics, the WS₂/IGZO heterojunction-based TFT show excellent and symmetrical ambipolar behavior, which can be attributed to the p-channel of WS₂ and n-channel of IGZO. Gate-induced holes in WS₂ will dominate the system's electrical conductivity after applying negative V_{gs} , the transistor shows p-type behavior. However, the positive V_{gs} induces the increment of electrons and finally leads to the transistor showing n-type behavior. In general, the emerging ambipolar properties with both p- and n-type conducting channels reveal great potential applications in future electronics and oscillator for the WS₂/IGZO heterojunction. The on/off current ratio of the WS₂/IGZO heterojunction-based TFT is 5090, this ratio degrades compared to the device based on IGZO which on/off current ratio is 25 530 (see Figure S1b). This is induced by the wet transfer process of CVD-WS₂, which enlarges the distance of the interface between WS₂ and IGZO.^{34,35} The mobility of transistors are obtained using $\mu = [L/(WC_i V_{ds})] \cdot [(dI_{ds}/dV_{gs})]$, where (dI_{ds}/dV_{gs}) is the slope of the linear region of transfer

curves, C_i is the gate capacitance of the gate insulator per unit area, L and W are the length and width of the channel, respectively ($L = 5 \mu\text{m}$ and $W = 20 \mu\text{m}$, as shown in Figure 1b).³⁶ The field-effect mobility increased from ~ 0.3 to $23.8 \text{ cm}^2/\text{V s}$ (see Figure S5b) after the WS₂ film is introduced.

3.2. Gas-Sensing Properties of WS₂/IGZO Heterojunction Chemiresistor Devices. The responses to NO₂ gas among WS₂-only, IGZO-only, and WS₂/IGZO-based device were investigated first. As shown in Figure 2a, WS₂-, IGZO-, and WS₂/IGZO-based sensor has $S_{WS_2} = 430\%$, $S_{IGZO} = -70\%$, and $S_{WS_2/IGZO} = 5470\%$ when exposed to 50 ppm NO₂, confirming that WS₂/IGZO has much better NO₂-sensing behavior than that of only WS₂ and IGZO. The superior gas-sensing performance could benefit from the heterojunction structure. However, three types of device have a very long recovery time, which might be related to chemical adsorption of NO₂ on the surface. Then, to evaluate the NO₂-sensing performance of the WS₂/IGZO heterojunction chemiresistor sensor, the dynamic current change was measured under different gas concentration of NO₂ ranging from 1 to 300 ppm.

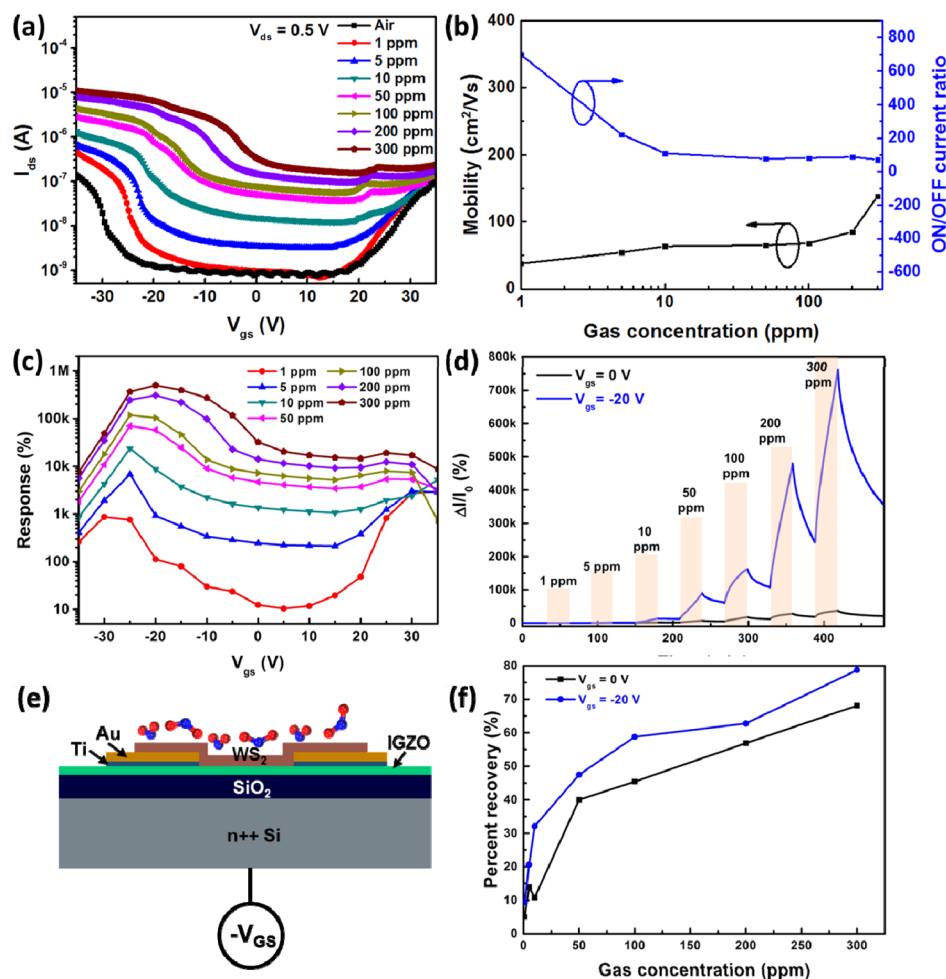


Figure 3. (a) Transfer curves of WS₂/IGZO TFT under different NO₂ concentrations. (b) Mobility and ON/OFF current ratio of devices under different NO₂ concentrations. (c) Gas response of the devices under different NO₂ concentrations after applying different gate biases. (d) Dynamic response of the device under different NO₂ concentrations at 0 and -20 V gate bias. (e) Schematic of WS₂/IGZO TFT under a negative gate bias. (f) Percent recovery of the device under different NO₂ concentrations at 0 and -20 V gate bias.

As shown in Figure 2b, with increasing gas concentration, the current of the device increases. The response of the device after exposure to different concentration NO₂ are shown in Figure 2c. It can be found that the lower the concentration, the longer recovery time needed. Thus, we unified the recovery time with 30 min for ease of comparison. The device presents high response (*S*) of 230% under 5 ppm and 18 170% under 300 ppm NO₂, which is much higher than that of ultra-thin WS₂ nanosheets (*S* = 9.3% @ 1 ppm NO₂) and WS₂ nanosheets decorated by Ag nanowires (*S* = 667% @ 500 ppm NO₂).^{12,13} Figure 2d shows the responses of the WS₂/IGZO heterojunction as a function of the NO₂ concentrations in 1 to 300 ppm. The experimental data were fitted by exponential function as

$$\text{Response } (S) = 648.28 \times C^{0.6} \quad (2)$$

where *C* is the gas concentration of NO₂. Also, the linear fitting results of log(*S*) versus log(*C*) (see the inset image of Figure 2d) further illustrates that the surface coverage of adsorbed NO₂ molecules follows Freundlich isotherm adsorption, which is the most important multisite adsorption isotherm for rough surfaces.³⁷ Besides, because the signal is three times greater than the noise, we calculated the LOD of the as-fabricated sensor according to the International Union of Pure and

Applied Chemistry (IUPAC). The theoretical LOD can be calculated from the slope of the linear region of the response curve and the root-mean-square (rms) deviation at the baseline, according to the equation

$$\text{LOD (ppb)} = 3 \times \text{rms}_{\text{noise}} / \text{slope} \quad (3)$$

where rms_{noise} is the standard deviation of noise and is calculated as 0.0023, according to 200 data points in the baseline of the response curve (Figure S7a,b). The calculated LOD for NO₂ is 29 ppb at RT, which is much better than the reported values.

In addition, the response and recovery kinetics are critical to the reliability and sustainability of the gas sensor. Thus, we quantitatively investigated the recovery characteristics of WS₂/IGZO-based gas sensors by calculating the percent recovery. The percent recovery is expressed as

$$\begin{aligned} \text{Percent recovery (\%)} \\ = (I_{g(V_{gs})} - I_{r(V_{gs})}) / (I_{g(V_{gs})} - I_{0(V_{gs})}) \times 100\% \end{aligned} \quad (4)$$

where *I*₀(*V*_{gs}) and *I*_g(*V*_{gs}) are the current value in dry air and after 30 min exposure to NO₂ gas under different *V*_{gs}, respectively. *I*_r(*V*_{gs}) is the recovered current value after exposure to dry air for 30 min under different *V*_{gs}. As shown in Figure 2e, the higher

Table 1. Comparison of Various Gas Sensor Materials with Respect to Reported NO₂ Ranges (ppm), LOD (ppm), Working Temperature (°C), and Response (%)

sensing materials	sensor type	NO ₂ (ppm)	LOD (ppm)	temperature (°C)	response (%)	ref
WS ₂ /IGZO	TFT	300	0.026	RT	499 400@-20 V _{gs}	this work
		5			6820@-25 V _{gs}	
WS ₂ nanosheets	chemiresistor	0.1	0.1	RT	9.3	12
WS ₂ /Ag	TFT	500		RT	667	13
WS ₂ /WO ₃	chemiresistor	100		150	1000	14
WS ₂ /ZnS heterostructure	chemiresistor	5	0.053	RT	3250	39
MoS ₂ /ZnO hetero-nanostructure	chemiresistor	5		RT	3035	40
monolayer MoS ₂	TFT	0.1	0.1	RT	50	41
<i>a</i> -IGZO ₄	chemiresistor	5		200	3300	42
photo-induced IGZO	TFT	5		RT	20	28

the gas concentration the larger the percent recovery, indicating that under a high NO₂ gas concentration the device can recover faster than when under low gas concentration. Under low NO₂ gas concentration, gas molecules are easily and mostly adsorbed by the edge sites and defects of the heterojunction and the interface.¹⁴ Because of the high adsorption energy of the edge sites and defects, the device recovers so slowly. With increasing gas concentration, most of the gas molecules are adsorbed by the surface of the WS₂/IGZO heterojunction, which easily escape from the adsorption site under airflow. Accordingly, we investigated the dynamic response of the device after 3 cycles under 50 ppm NO₂. Here, the device was exposed to 50 ppm NO₂ for 30 min, and then with the flow of dry air for 90 min to make the sensor fully recovered. As shown in Figure 2f, the result shows that the chemiresistor sensor has good repeatability.

To study the selectivity, we measured the responses of the device to several other gases, including a reducing gas NH₃ (100 ppm) oxidizing gases of CO (100 ppm). As shown in Figure S9, the sensor response toward NH₃ and CO under 100 ppm are -137 and 94%, respectively, which are far lower than that of NO₂. Then, the device was measured under different humidity environments (with a relative humidity of 10, 30, 50, 65, and 80%). The sensor presents the maximum response of 33% (see Figure S10). It is much less than that toward NO₂, indicating that humidity has slight effects on the gas-sensing performance toward NO₂. Accordingly, it can be concluded that the WS₂/IGZO heterojunction has good selectivity, sensitivity, low operation temperature, and unaffected by the RH of environments.

3.3. Gas-Sensing Properties of WS₂/IGZO TFT. The semiconducting behavior is attractive to enhance sensing performance according to its tunable transport characteristics after exposure to light or gate bias.^{17,38} Thus, we investigated the sensing behavior of the WS₂/IGZO TFT under different NO₂ gas concentrations after applying different gate biases. Figure 3a shows the transfer characteristics of the device under air and increasing NO₂ gas concentration. It can be found that by applying the gate bias, the response of the as-fabricated gas sensor was modulated by the carrier concentration. Along with increasing the NO₂ gas concentration, more electrons are accepted by the WS₂/IGZO vertical stacked heterojunction, the hole current from the WS₂ will gradually strengthen. Notably, when the concentration is higher than 50 ppm, the tunable polarity behaviors ranging from ambipolar to p-type behavior is observed. Because more and more NO₂ gas molecules are adsorbed by the surface of WS₂, the current in the p-channel of WS₂ increases obviously and dominates the

electrical transport. Thus, the transistor shows debilitate ambipolar behavior and distinct p-type characteristics. As shown in Figure 3b, the electrical properties of the devices are tunable under different gas concentrations. When the gas concentration of NO₂ increases, the mobility of the TFT increase and reaches to 138 cm²/V s under 300 ppm; while the on/off ratio decreases from 696 (1 ppm) to 72 (300 ppm).

Figure 3c shows the response of the WS₂/IGZO transistors toward different concentrations of NO₂, which were measured at fixed V_{gs} ranging from -35 to 35 V with a step of 5 V. After exposure to different NO₂ concentrations, the maximum response occurs at different gating potentials depending on the gas concentrations. The gating potential-dependence behavior is mainly induced by the gas doping effects, which modifies the operation ranges of the transistor compared with the regime for the same gate bias under an air atmosphere. For instance, at high concentrations (200–300 ppm), with a gating voltage of -20 V, the transistor is nearly on the saturation regime while under air at the same gate bias the transistors are on the linear regime. At low concentrations, the maximum responses are obtained with a gating tension larger than -20 V because the TFT is in the linear regime. In all cases, for a more negative gate bias, the responses decrease because the transistor is operational in the saturation regime with and without NO₂ gas molecules. Figure 3d shows that the response of the device is improved to be 499 400% at 300 ppm, and the recovery time is shortened after applying -20 V gate bias. As shown in Figure 3f, the higher the gas concentration the larger the percent recovery, which is similar to that of WS₂/IGZO heterojunction chemiresistor devices. However, the TFT gas sensor has a higher percent recovery, indicating that the surface activity can be enhanced under gate voltage. The gas-sensing performance is much higher than that of WS₂-based, MoS₂-based, and IGZO-based TFT gas sensors (see Table 1). The results illustrated that WS₂/IGZO TFT is also a promising candidate for the NO₂ gas sensor. To the best of our knowledge, the TFT device has the best NO₂ gas sensor response compared to all the gas sensors based on TMDC materials.

3.4. Gas-Sensing Mechanism. When WS₂ is combined with the IGZO, the p-N type WS₂/IGZO heterojunctions are formed, inducing a different electron transport mechanism from that of individual WS₂ and IGZO. The band diagrams of WS₂ and IGZO before and after equilibrium are shown in Figure 1d,e. IGZO has a higher work function (*W*) of 7.01 eV compared to WS₂ (5.89 eV), and a higher *E_f* compared to that of WS₂. Thus, electrons flow from IGZO to WS₂ while holes from WS₂ to IGZO, until their *E_f* align, resulting in the energy

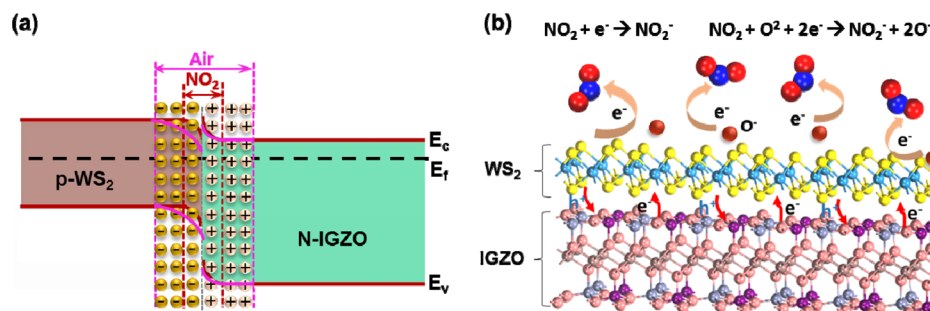


Figure 4. (a) Energy band structure of the WS₂/IGZO heterojunction in air and a NO₂ atmosphere and (b) schematic of sensing mechanisms of the WS₂/IGZO heterojunction to NO₂ molecules.

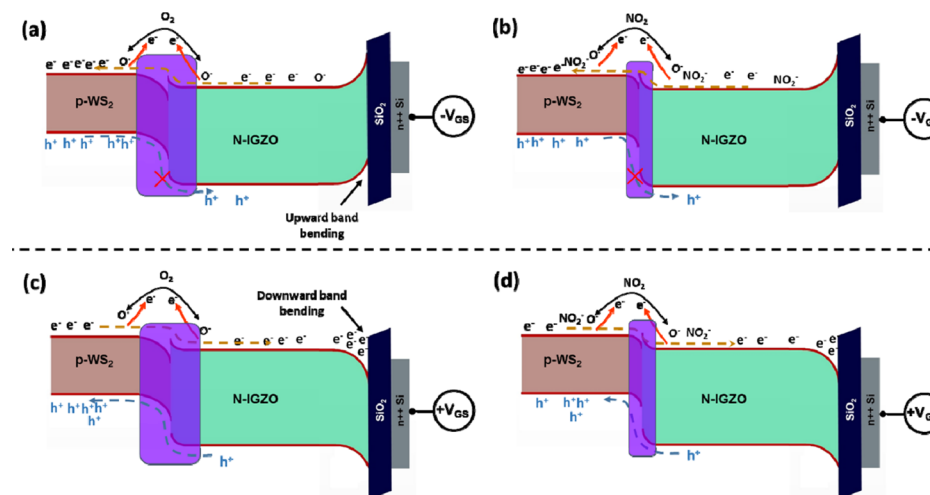


Figure 5. After applying negative V_{gs} , the band diagram of WS₂/IGZO TFT (a) in air and (b) a NO₂ atmosphere. After applying positive V_{gs} , the band diagram of WS₂/IGZO TFT (c) in air and (d) a NO₂ atmosphere. The purple region represents depletion layer.

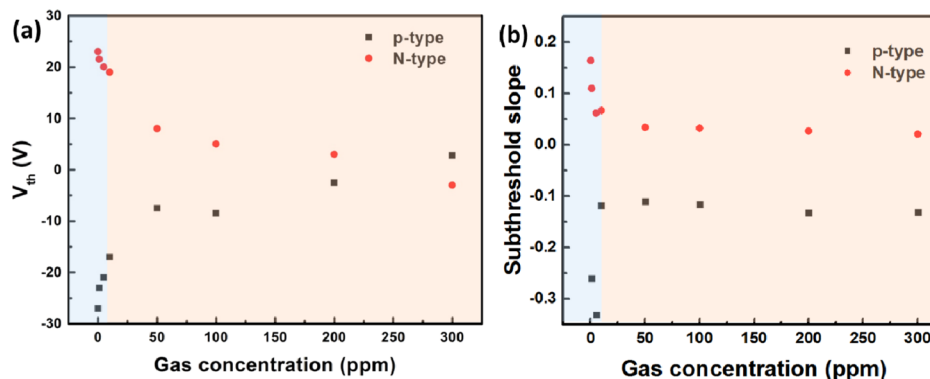


Figure 6. WS₂/IGZO sensing mechanism study. (a) Threshold voltage (V_{th}) and (b) subthreshold slope (K_{th}) vs gas concentrations for NO₂.

band bending in the depletion region at the interface between WS₂ and IGZO.⁴³ As shown in Figure 4a, the region beneath the p-N interface creates an internal electric field, which acts as a potential barrier for further carrier diffusion.⁴⁰ The potential barriers and depletion layers contribute to the low conductivity of the WS₂/IGZO heterojunction in air. As shown in Figure 4b, when the sensor is exposed to air, oxygen species are adsorbed on the surface and interface layer of WS₂/IGZO heterojunctions. Then, oxygen molecules can easily trap the free electrons from their conduction band (E_c) to form ionic oxygen species (O_2^- or O^-).⁴⁴ When the sensor is exposed to NO₂, the oxidizing NO₂ reacts with ionic oxygen species as well as adsorbed on the surface of heterojunctions. The

adsorbed NO₂ molecules attract the electrons from the heterojunction, produce NO_3^- or NO_2^- , and decrease its carrier concentration. The built-in electric field is non-equilibrium, inducing extra holes slip from the IGZO and accumulate at the surface of WS₂, and the width of the heterojunction barrier decreases. It also leads to a decrease of the depletion layer thickness, and an increase of the conductivity of the device consequently.

In general, the band shape and barrier height of the heterojunction can be effectively modulated by applying an external gate voltage on the back-gate silicon electrode.^{45–48} As shown in Figure 5a,b, the N-IGZO has a large number of electrons, the electron drifts from IGZO to WS₂ to overcome

the WS₂/IGZO barrier under a constant positive V_{ds} . With a negative V_{gs} , the electron concentrations of IGZO near the SiO₂ dielectric substrate decrease, which induces the E_c of IGZO decrease according to the equation of electron concentrations,⁴⁹ $n_0 = N_c \times \exp(-(E_c - E_F)/k_0T)$, where N_c is the effective density of states of the conduction band, k_0 is the Boltzmann constant, T is the temperature, and results in the upward band bending between the SiO₂ and IGZO films. On the contrary, after applying a positive V_{gs} , the electron concentration in IGZO increase near the SiO₂ substrate and shift the Fermi level downward, forming a downward band bending (see Figure 5c,d). Therefore, the junction effect and gate-induced band bending dominate the electrical transport and lead to the ambipolar behaviors. When the TFT exposures to the NO₂ gas, the adsorption energy and charge transfer between gas molecules and the WS₂/IGZO heterojunction increases obviously due to the effects of the external electric field from the back gate voltage.^{50,51} Thus, the depletion layer thickness of TFT decreases greater than that in chemiresistor mode, and the current of heterojunction increases with the rising back gate voltage.

Moreover, the conductivity of the TFT increase with increasing gas concentration, a lateral shift of V_{th} and a change of the subthreshold slope can be observed, as shown in Figures 3a and 6a. Usually, chemical doping by gas molecules can induce large charge transfer between the sensing materials and dopant, and finally lead to current increase and V_{th} shift in a TFT-type gas sensor.^{52,53} For as-fabricated WS₂/IGZO TFT, the transfer curves of p-type behavior shift toward the positive gate voltage direction, while the n-type behavior toward the negative direction. It is mainly attributed to the high gas doping effects on the WS₂/IGZO heterojunction, which leads to large charge transfer between gas molecules and heterojunction. Thus, the device is difficult to go back to off-state under high gas concentration, and the on/off ratio decreases (see Figure 3a,b). Moreover, because the WS₂ film at the top layer of the vertically stacking WS₂/IGZO heterojunction, most of the NO₂ gas molecules can be adsorbed by p-channel WS₂ at first. It results in high current density inside WS₂, and the device presents enhanced p-type behavior.

A change of subthreshold slope is usually found in a TFT with a metal/semiconductor contact because its Schottky barrier height can be modulated by gas concentration.^{54,55} The WS₂/IGZO heterojunction TFT's subthreshold slope ($K_{th} = dV_{gs}/d\log(I_{ds})$) for both p- and n-type behavior decrease sharply from 0 to 10 ppm and then increase slightly when the gas concentration is higher than 50 ppm. These results can be attributed to two types of sensing mechanism: Schottky barrier modulation and doping of the transistor channel. As shown in Figure 6b, when the device exposures to low NO₂ gas concentration, the adsorption sites are sufficient for detecting many gas molecules, thus a Schottky barrier build-up between the WS₂, IGZO, and metal in the contact region is changed obviously and so does the K_{th} . For a high NO₂ gas concentration, the adsorption sites reach saturation which induces slight changes in K_{th} and V_{th} . Both shift of the V_{th} and changes of the K_{th} can be associated to the fact that the sensing mechanism of the WS₂/IGZO transistor is affected by the doped of NO₂ and the modulated Schottky barrier value at the WS₂ and IGZO with a metal contact interface. Therefore, with the increase in the concentration of NO₂, more charges are transferred to the heterojunction, and the WS₂/IGZO heterojunction-based sensor shows a ultrahigh response to

NO₂ under gate voltage. The proposed sensing mechanism is in agreement with the fact that the device is more difficult to recover at low concentrations, as is previously mentioned, the metal electrode interfaces and the edges are more favorable for binding NO₂ molecules, the molecules adsorbed in the metal electrode interface with the junctions will contribute to the Schottky barrier modulation while those located at edges will contribute to the doping because both kinds of sites possess a higher binding energy, these molecules will be more difficult to desorb. However, in order to clearly identify where the predominant gas-sensing behavior is taking place, further studies must be performed, it might be interesting to analyze the gas response and the recovery time with a passivate device in the interface between the metal electrodes and the heterojunction, and compare with response with a passivate device in the channel (where just the metal electrode area is exposed).

4. CONCLUSIONS

In this work, the gas-sensing performances of as-fabricated CVD-WS₂/IGZO heterojunction-based devices were investigated in two modes, chemiresistor and TFT modes. The as-fabricated gas sensor has a maximum response of 18 170% on the chemiresistor mode, and 499 400% on the TFT mode under 300 ppm NO₂ after applying -20 V gate bias. It is much better than that of only WS₂ and IGZO. Moreover, the sensor shows excellent gas selectivity toward NO₂ with comparison to several gas vapors such as CO, NH₃, and humidity. The superior gas-sensing performance could benefit from the heterojunction of WS₂ and IGZO, and the external electric field under back gate voltage. In addition, the transistor notably presents a typical ambipolar-behavior under dry air, while the transistor becomes p-type as the amount of NO₂ increases. The mobility, on/off ratio, and subthreshold slope of the device is modulated by the NO₂ gas concentration. The unique tunable behavior can be associated to the doping effects of NO₂ on the heterojunction and the modulated Schottky barrier value at the WS₂ and IGZO with a metal contact interface. Consequently, the WS₂/IGZO-based device is a potential candidate for the NO₂ gas sensor and tunable engineering application. However, the device has long recovery time which needs to be improved for future work, such as attaching functional groups or applying UV illumination. Besides, the long-term response stability is important for practical application, which we will deeply study in our future works.

■ ASSOCIATED CONTENT

Supporting Information

The Supporting Information is available free of charge on the ACS Publications website at DOI: 10.1021/acsami.9b13773.

Transfer characteristics of WS₂ and IGZO transistor; experimental setup used for gas-sensing measurements; AFM, Raman, and PL image of WS₂, IGZO, and WS₂/IGZO heterojunction; I - V characteristics of the individual WS₂ and IGZO; Mott-Schottky plot for p-WS₂; response of IGZO, WS₂, and WS₂/IGZO devices; calculation of LOD; and response of different types of gas molecules (PDF)

AUTHOR INFORMATION

Corresponding Authors

*E-mail: h.ye@tudelft.nl (H.Y.).

*E-mail: rentl@tsinghua.edu.cn (T.-L.R.).

*E-mail: G.Q.Zhang@tudelft.nl (G.Z.).

ORCID

Hongyu Tang: 0000-0002-2720-6709

Yutao Li: 0000-0002-0665-0683

Leandro Sacco: 0000-0002-5384-2020

He Tian: 0000-0001-7328-2182

Author Contributions

H.T. and Y.L. contributed equally to this work. H.T. proposed the concept, designed and fabricated the device, performed the experiments, and contributed to the writing of the paper. Y.L. proposed the designed and fabricated the device, and contributed to the writing of the paper. R.S. discussed the gas testing experiments and contributed to the writing of the paper. L.S. contributed to the gas-sensing mechanism analysis and the writing of the paper. H.Z. performed the gas-sensing experiments. H.Y., H.Y., and X.F. provided valuable discussion. Finally, T.-L.R. and G.Z. provided guidance to the research. All authors discussed the results and commented on the manuscript.

Notes

The authors declare no competing financial interest.

ACKNOWLEDGMENTS

We thank Dr. Boyao Zhang in Delft University of Technology for her vigorous help of Mott–Schottky measurement, and we also thank Dr. Jinming Jian in Tsinghua University, and Dr. Jianwen Sun in Delft University of Technology for their helpful discussions. This work was supported by Guangdong Science and Technology Department (China) (no. 2019B010126001), the National Natural Science Foundation of China under grant no. 51706029, and the National Key Research and Development Program of China under grant no.2018YFE0204600).

REFERENCES

- (1) Hu, Y.; Huang, Y.; Tan, C.; Zhang, X.; Lu, Q.; Sindoro, M.; Huang, X.; Huang, W.; Wang, L.; Zhang, H. Two-dimensional transition metal dichalcogenide nanomaterials for biosensing applications. *Mater. Chem. Front.* **2017**, *1*, 24–36.
- (2) Khalil, H. M. W.; Khan, M. F.; Eom, J.; Noh, H. Highly stable and tunable chemical doping of multilayer WS₂ field effect transistor: Reduction in contact resistance. *ACS Appl. Mater. Interfaces* **2015**, *7*, 23589–23596.
- (3) Lan, C.; Li, C.; Yin, Y.; Liu, Y. Large-area synthesis of monolayer WS₂ and its ambient-sensitive photo-detecting performance. *Nano-scale* **2015**, *7*, 5974–5980.
- (4) Choi, W.; Choudhary, N.; Han, G. H.; Park, J.; Akinwande, D.; Lee, Y. H. Recent development of two-dimensional transition metal dichalcogenides and their applications. *Mater. Today* **2017**, *20*, 116–130.
- (5) Manzeli, S.; Ovchinnikov, D.; Pasquier, D.; Zayzev, O. V.; Kis, A. 2D transition metal dichalcogenides. *Nat. Rev. Mater.* **2017**, *2*, 17033.
- (6) Yun, Y. J.; Hong, W. G.; Choi, N.-J.; Kim, B. H.; Jun, Y.; Lee, H.-K. Ultrasensitive and highly selective graphene-based single yarn for use in wearable gas sensor. *Sci. Rep.* **2015**, *5*, 10904.
- (7) Mehew, J. D.; Unal, S.; Torres Alonso, E.; Jones, G. F.; Fadhil Ramadhan, S.; Craciun, M. F.; Russo, S. Fast and Highly Sensitive Ionic-Polymer-Gated WS₂–Graphene Photodetectors. *Adv. Mater.* **2017**, *29*, 1700222.
- (8) Wang, G.; Li, L.; Fan, W.; Wang, R.; Zhou, S.; Lü, J.-T.; Gan, L.; Zhai, T. Interlayer Coupling Induced Infrared Response in WS₂/

MoS₂ Heterostructures Enhanced by Surface Plasmon Resonance. *Adv. Funct. Mater.* **2018**, *28*, 1800339.

(9) Kang, K.; Godin, K.; Kim, Y. D.; Fu, S.; Cha, W.; Hone, J.; Yang, E.-H. Graphene-Assisted Antioxidation of Tungsten Disulfide Monolayers: Substrate and Electric-Field Effect. *Adv. Mater.* **2017**, *29*, 1603898.

(10) Bui, V. Q.; Pham, T.-T.; Le, D. A.; Thi, C. M.; Le, H. M. A first-principles investigation of various gas (CO, H₂O, NO, and O₂) absorptions on a WS₂ monolayer: stability and electronic properties. *J. Phys.: Condens. Matter* **2015**, *27*, 305005.

(11) Zhou, C. J.; Yang, W. H.; Wu, Y. P.; Lin, W.; Zhu, H. L. Theoretical study of the interaction of electron donor and acceptor molecules with monolayer WS₂. *J. Phys. D: Appl. Phys.* **2015**, *48*, 285303.

(12) Xu, T.; Liu, Y.; Pei, Y.; Chen, Y.; Li, X. The ultra-high NO₂ response of ultra-thin WS₂ nanosheets synthesized by hydrothermal and calcination processes. *Sens. Actuators, B* **2018**, *259*, 789–796.

(13) Ko, K. Y.; Song, J.-G.; Kim, Y.; Choi, T.; Shin, S.; Lee, C. W.; Lee, K.; Koo, J.; Lee, H.; Kim, J.; Lee, T.; Park, J.; Kim, H. Improvement of Gas-Sensing Performance of Large-Area Tungsten Disulfide Nanosheets by Surface Functionalization. *ACS Nano* **2016**, *10*, 9287–9296.

(14) Perrozzi, F.; Emamjomeh, S. M.; Paolucci, V.; Taglieri, G.; Ottaviano, L.; Cantalini, C. Thermal stability of WS₂ flakes and gas sensing properties of WS₂/WO₃ composite to H₂, NH₃ and NO₂. *Sens. Actuators, B* **2017**, *243*, 812–822.

(15) Zhu, X.; Monahan, N. R.; Gong, Z.; Zhu, H.; Williams, K. W.; Nelson, C. A. Charge transfer excitons at van der Waals interfaces. *J. Am. Chem. Soc.* **2015**, *137*, 8313–8320.

(16) Yan, W.; Worsley, M. A.; Pham, T.; Zettl, A.; Carraro, C.; Maboudian, R. Effects of ambient humidity and temperature on the NO₂ sensing characteristics of WS₂/graphene aerogel. *Appl. Surf. Sci.* **2018**, *450*, 372–379.

(17) Tabata, H.; Sato, Y.; Oi, K.; Kubo, O.; Katayama, M. Bias-and Gate-Tunable Gas Sensor Response Originating from Modulation in the Schottky Barrier Height of a Graphene/MoS₂ van der Waals Heterojunction. *ACS Appl. Mater. Interfaces* **2018**, *10*, 38387–38393.

(18) Bae, G.; Jeon, I. S.; Jang, M.; Song, W.; Myung, S.; Lim, J.; Lee, S. S.; Jung, H.-K.; Park, C.-Y.; An, K.-S. Complementary Dual-Channel Gas Sensor Devices Based on a Role-Allocated ZnO/Graphene Hybrid Heterostructure. *ACS Appl. Mater. Interfaces* **2019**, *11*, 16830–16837.

(19) Kim, K. S.; Ahn, C. H.; Jung, S. H.; Cho, S. W.; Cho, H. K. Toward adequate operation of amorphous oxide thin film transistors for low concentration gas detection. *ACS Appl. Mater. Interfaces* **2018**, *10*, 10185–10193.

(20) Jeong, H.-S.; Park, M.-J.; Kwon, S.-H.; Joo, H.-J.; Kwon, H.-I. Highly sensitive and selective room-temperature NO₂ gas-sensing characteristics of SnOX-based p-type thin-film transistor. *Sens. Actuators, B* **2019**, *288*, 625–633.

(21) Kim, K. S.; Ahn, C. H.; Jung, S. H.; Cho, S. W.; Cho, H. K. Toward Adequate Operation of Amorphous Oxide Thin-Film Transistors for Low-Concentration Gas Detection. *ACS Appl. Mater. Interfaces* **2018**, *10*, 10185–10193.

(22) Zan, H.-W.; Yeh, C.-C.; Meng, H.-F.; Tsai, C.-C.; Chen, L.-H. Achieving high field-effect mobility in amorphous indium-gallium-zinc oxide by capping a strong reduction layer. *Adv. Mater.* **2012**, *24*, 3509–3514.

(23) Wang, Y.; Yang, J.; Wang, H.; Zhang, J.; Li, H.; Zhu, G.; Shi, Y.; Li, Y.; Wang, Q.; Xin, Q. Amorphous-InGaZnO thin-film transistors operating beyond 1 GHz achieved by optimizing the channel and gate dimensions. *IEEE Trans. Electron Devices* **2018**, *65*, 1377–1382.

(24) Godo, H.; Kawae, D.; Yoshitomi, S.; Sasaki, T.; Ito, S.; Ohara, H.; Kishida, H.; Takahashi, M.; Miyayaga, A.; Yamazaki, S. Temperature Dependence of Transistor Characteristics and Electronic Structure for Amorphous In–Ga–Zn-Oxide Thin Film Transistor. *Jpn. J. Appl. Phys.* **2010**, *49*, 03CB04.

(25) Kim, D. H.; Choi, S.-H.; Cho, N. G.; Chang, Y.; Kim, H.-G.; Hong, J.-M.; Kim, I.-D. High stability InGaZnO₄ thin-film transistors

using sputter-deposited PMMA gate insulators and PMMA passivation layers. *Electrochem. Solid-State Lett.* **2009**, *12*, H296–H298.

(26) Yao, R.; Zheng, Z.; Xiong, M.; Zhang, X.; Li, X.; Ning, H.; Fang, Z.; Xie, W.; Lu, X.; Peng, J. Low-temperature fabrication of sputtered high-k HfO₂ gate dielectric for flexible a-IGZO thin film transistors. *Appl. Phys. Lett.* **2018**, *112*, 103503.

(27) Suresh, A.; Muth, J. F. Bias stress stability of indium gallium zinc oxide channel based transparent thin film transistors. *Appl. Phys. Lett.* **2008**, *92*, 033502.

(28) Knobelspies, S.; Bierer, B.; Daus, A.; Takabayashi, A.; Salvatore, G.; Cantarella, G.; Ortiz Perez, A.; Wöllenstein, J.; Palzer, S.; Tröster, G. Photo-Induced Room-Temperature Gas Sensing with a-IGZO Based Thin-Film Transistors Fabricated on Flexible Plastic Foil. *Sensors* **2018**, *18*, 358.

(29) Ramezanzadeh, B.; Bahlakeh, G.; Mohamadzadeh Moghadam, M. H.; Mirafteb, R. Impact of size-controlled p-phenylenediamine (PPDA)-functionalized graphene oxide nanosheets on the GO-PPDA/Epoxy anti-corrosion, interfacial interactions and mechanical properties enhancement: Experimental and quantum mechanics investigations. *Chem. Eng. J.* **2018**, *335*, 737–755.

(30) Butanovs, E.; Vlassov, S.; Kuzmin, A.; Piskunov, S.; Butikova, J.; Polyakov, B. Fast-response single-nanowire photodetector based on ZnO/WS₂ core/shell heterostructures. *ACS Appl. Mater. Interfaces* **2018**, *10*, 13869–13876.

(31) Tak, Y. J.; Kim, D. J.; Kim, W.-G.; Lee, J. H.; Kim, S. J.; Kim, J. H.; Kim, H. J. Boosting Visible Light Absorption of Metal-Oxide-Based Phototransistors via Heterogeneous In–Ga–Zn–O and CH₃NH₃PbI₃ Films. *ACS Appl. Mater. Interfaces* **2018**, *10*, 12854–12861.

(32) Tonti, D.; Varsano, F.; Decker, F.; Ballif, C.; Regula, M.; Remškar, M. Preparation and photoelectrochemistry of semiconducting WS₂ thin films. *J. Phys. Chem. B* **1997**, *101*, 2485–2490.

(33) Devadasan, J. J.; Sanjeeviraja, C.; Jayachandran, M. Electrodeposition of p-WS₂ thin film and characterisation. *J. Cryst. Growth* **2001**, *226*, 67–72.

(34) Park, J.-S.; Jeong, J. K.; Chung, H.-J.; Mo, Y.-G.; Kim, H. D. Electronic transport properties of amorphous indium-gallium-zinc oxide semiconductor upon exposure to water. *Appl. Phys. Lett.* **2008**, *92*, 072104.

(35) Yang, J.; Kwak, H.; Lee, Y.; Kang, Y.-S.; Cho, M.-H.; Cho, J. H.; Kim, Y.-H.; Jeong, S.-J.; Park, S.; Lee, H.-J.; Kim, H. MoS₂–InGaZnO Heterojunction Phototransistors with Broad Spectral Responsivity. *ACS Appl. Mater. Interfaces* **2016**, *8*, 8576–8582.

(36) Lim, S. H.; Kim, J.; Lee, S.-g.; Kim, Y. S. Water-soluble polymer dielectric with potential for high performance organic thin-film transistors. *Chem. Commun.* **2010**, *46*, 3961–3963.

(37) Freundlich, H. *Kapillarchemie, eine Darstellung der Chemie der Kolloide und verwandter Gebiete*; akademische Verlagsgesellschaft, 1909.

(38) Park, S.; An, S.; Mun, Y.; Lee, C. UV-enhanced NO₂ gas sensing properties of SnO₂-core/ZnO-shell nanowires at room temperature. *ACS Appl. Mater. Interfaces* **2013**, *5*, 4285–4292.

(39) Han, Y.; Liu, Y.; Su, C.; Wang, S.; Li, H.; Zeng, M.; Hu, N.; Su, Y.; Zhou, Z.; Wei, H.; Yang, Z. Interface engineered WS₂/ZnS heterostructures for sensitive and reversible NO₂ room temperature sensing. *Sens. Actuators, B* **2019**, *296*, 126666.

(40) Han, Y.; Huang, D.; Ma, Y.; He, G.; Hu, J.; Zhang, J.; Hu, N.; Su, Y.; Zhou, Z.; Zhang, Y.; Yang, Z. Design of Heteronanostructures on MoS₂ Nanosheets to Boost NO₂ Room Temperature Sensing. *ACS Appl. Mater. Interfaces* **2018**, *10*, 22640–22649.

(41) Liu, B.; Chen, L.; Liu, G.; Abbas, A. N.; Fathi, M.; Zhou, C. High-performance chemical sensing using Schottky-contacted chemical vapor deposition grown monolayer MoS₂ transistors. *ACS Nano* **2014**, *8*, 5304.

(42) Yang, D. J.; Whitfield, G. C.; Cho, N. G.; Cho, P.-S.; Kim, I.-D.; Saltsburg, H. M.; Tuller, H. L. Amorphous InGaZnO₄ films: Gas sensor response and stability. *Sens. Actuators, B* **2012**, *171–172*, 1166–1171.

(43) Bhattacharya, P.; Pang, L. Y. *Semiconductor Optoelectronic Devices*; Prentice Hall: Upper Saddle River, NJ, 1997; Vol. 613.

(44) Deng, Y. *Semiconducting Metal Oxides for Gas Sensing*; Springer, 2019.

(45) Roy, T.; Liu, L.; de la Barrera, S.; Chakrabarti, B.; Hesabi, Z. R.; Joiner, C. A.; Feenstra, R. M.; Gu, G.; Vogel, E. M. Tunneling characteristics in chemical vapor deposited graphene–hexagonal boron nitride–graphene junctions. *Appl. Phys. Lett.* **2014**, *104*, 123506.

(46) Huo, N.; Yang, J.; Huang, L.; Wei, Z.; Li, S.-S.; Wei, S.-H.; Li, J. Tunable Polarity Behavior and Self-Driven Photoswitching in p-WS₂/n-WS₂ Heterojunctions. *Small* **2015**, *11*, 5430–5438.

(47) Tang, H.; Tan, C.; Yang, H.; Zheng, K.; Li, Y.; Ye, H.; Chen, X.; Fan, X.; Ren, T.; Zhang, G. Tunable electronic and optical properties of the WS₂/IGZO heterostructure via an external electric field and strain: a theoretical study. *Phys. Chem. Chem. Phys.* **2019**, *21*, 14713–14721.

(48) Evtukh, A.; Hartnagel, H.; Yilmazoglu, O.; Mimura, H.; Pavlidis, D. *Vacuum Nanoelectronic Devices: Novel Electron Sources and Applications*; John Wiley & Sons, 2015.

(49) Seeger, K. *Semiconductor Physics*; Springer Science & Business Media, 2013.

(50) Liang, X.-Y.; Ding, N.; Ng, S.-P.; Wu, C.-M. L. Adsorption of gas molecules on Ga-doped graphene and effect of applied electric field: A DFT study. *Appl. Surf. Sci.* **2017**, *411*, 11–17.

(51) Li, H.; Yin, Z.; He, Q.; Li, H.; Huang, X.; Lu, G.; Fam, D. W. H.; Tok, A. I. Y.; Zhang, Q.; Zhang, H. Fabrication of single- and multilayer MoS₂ film-based field-effect transistors for sensing NO at room temperature. *Small* **2012**, *8*, 63–67.

(52) Kong, J.; Franklin, N. R.; Zhou, C.; Chapline, M. G.; Peng, S.; Cho, K.; Dai, H. Nanotube molecular wires as chemical sensors. *Science* **2000**, *287*, 622–625.

(53) Kim, S.; Lee, G.; Kim, J. Chemical Doping Effects of Gas Molecules on Black Phosphorus Field-Effect Transistors. *ECS J. Solid State Sci. Technol.* **2018**, *7*, Q3065–Q3069.

(54) Auvray, S.; Borghetti, J.; Goffman, M. F.; Filoramo, A.; Derycke, V.; Bourgoin, J. P.; Jost, O. Carbon nanotube transistor optimization by chemical control of the nanotube–metal interface. *Appl. Phys. Lett.* **2004**, *84*, 5106–5108.

(55) Bondavalli, P.; Legagneux, P.; Pribat, D. Carbon nanotubes based transistors as gas sensors: state of the art and critical review. *Sens. Actuators, B* **2009**, *140*, 304–318.